Chapter 8

Relocation of a global earthquake data set with a 3-D velocity model

We have relocated a global earthquake data set of 450,000 events contained in the International Seismological Centre (ISC), National Earthquake Information Center (NEIC), Europe-Mediterranean Seismological Centre (EMSC) and regional network data bases. The initial earthquake locations were obtained using a standard 1-D Earth reference model while the earthquake relocations presented in this study were performed in a highly detailed 3-D velocity model based on travel time tomography using a directed grid search technique. Tests with well-located events show an improvement of the earthquake location errors using the 3-D model with respect to a 1-D Earth reference model. Furthermore, systematic source parameter shifts of the events in the global earthquake data set can be observed with respect to their initial location which are caused by 3-D Earth structure now accounted for in the earthquake location process.

8.1 Introduction

Accurate earthquake locations are important not only for seismo-tectonic and seismic hazard assessment but also for the Comprehensive Nuclear Test-Ban Treaty (CTBT) or for tomography studies investigating the velocity structure of the Earth's crust and mantle. The accuracy of event locations depends on many factors among which are the number of phases used for computation of the location, proper phase identification, the velocity model used for computation of reference travel times and the location method itself. Besides the ISC and NEIC, which provide global data sets of earthquake locations, the updated EHB catalog of Engdahl *et al.* (1998) provides a groomed version of the ISC and NEIC bulletins from 1964 to 2004 including improvements compared to other global catalogs. The earthquake locations in the EHB catalog were obtained using a 1-D Earth reference model adding regionally averaged travel time corrections for upper mantle structure. Furthermore, phase identification of depth phases in this catalog was improved using probability density functions of later-arriving phases. The 3-D velocity heterogeneities in the source regions and along the ray paths of the

observed phases are not routinely taken into account in any of the earthquake locations provided by the mentioned global catalogs as it is computationally expensive and requires a good 3-D velocity model of the Earth's interior.
In this study, a highly detailed 3-D model obtained from travel time tomography will be used in a directed grid search to find more accurate earthquake locations for a global earthquake data set.

8.2 The earthquake data set

8.2.1 EHB catalog

The main data source is the reprocessed and updated earthquake catalog of Engdahl *et al.* (1998) which is based on the ISC bulletins and extended with data from the NEIC of the U.S. Geological Survery for the most recent events. This database will be referred to hereafter as EHB catalog. It contains earthquake observations for the period 1964–2004 including over 445,000 events with 27.4 million first and later arriving phases. The processing of Engdahl *et al.* (1998) comprised a phase re-identification, theoretical travel time calculation in the Earth reference model ak135 (Kennett *et al.*, 1995) and a source relocation taking into account regionally averaged travel time corrections for teleseismic phases.

8.2.2 Euro-Mediterranean bulletin

The Euro-Mediterranean bulletin of the EMSC provides the second data set used here. This bulletin contains a collection of travel time observations from local networks in the Euro-Mediterranean region (Godey *et al.*, 2006). Well-constrained earthquakes in this catalog were relocated by the EMSC. However, if existent, the corresponding EHB location is used here instead of the EMSC locations. Otherwise, the events are relocated in ak135 including regional patch corrections for consistency with the EHB catalog using the relocation method described in Section 8.3. The resulting EMSC subset then consists of over 96,000 additional first-arriving P and S phases from 9,700 events for the period 1998–2003 for which EHB locations could be found and 138,000 P and S arrival times for 6,400 events for which an EMSC location exists. Depth phases (pP, sP, pwP) were not used to avoid problems with phase misidentifications.

8.2.3 Newly picked data for stations in North America

Sandoval *et al.* (2004a) obtained waveform registrations from the Advanced National Seismic Network (ANSS), the Incorporated Research Institutions for Seismology (IRIS), Canadian National Seismic Network (CNSN), Southern California Earthquake Data Center (SCEDC) and the NARS-Baja project (Trampert *et al.*, 2003). For 486 events registered between 2002 and 2004, for which an EHB location existed, 120,000 P arrival times were picked by Sandoval *et al.* (2004a) with an automatic picking method. For most of these stations, arrival times were not determined before.

8.2.4 Newly picked data for stations in Europe

Additionally, temporary experiments with spatially dense station arrays in Europe, the ORFEUS (Observatories and Research Facilities for European Seismology) archives and a collection of registrations for the UK, Ireland and part of northwestern France provided to us by Arrowsmith (2003), form another source of data. The temporary experiment data comprise the SVEKALAPKO experiment in Finland (Bock et al., 2001), the TOR experiment in South Sweden, Denmark and North Germany (Gregersen *et al.*, 2002)), the EIFEL experiment in the Eifel (Ritter *et al.*, 2000), the CALIXTO experiment in Romania (Wenzel *et al.*, 1998) and the MIDSEA project with a number of stations surrounding the Mediterranean Sea (van der Lee *et al.*, 2001). The data from these stations were obtained as waveforms and arrival times were determined with the method of Sandoval *et al.* (2004a) resulting in a total of 86,600 P and S arrival times for 3100 events, for which an EHB location could be found.

8.3 Relocation method

From the EHB catalog, only events are relocated which are also relocated by Engdahl *et al.* (1998) and earthquakes which had a fixed EHB hypocenter depth are kept at fixed depth. Furthermore, we use only those P, S, pP, pwP, sP, PKPdf and PKiKP phases from the EHB data set, which were also used by Engdahl *et al.* (1998) for relocation and the additional phases from the other data sets for according EHB events. The additional EMSC events without corresponding EHB location are relocated using P and S phases. For all additional data, regional phases with absolute travel time residuals > 7.5 s and teleseismic phases with an absolute travel time residual > 3.5 s are not used. Also epicentral distances for P phases are limited to $< 100^\circ$ and for S to $< 80^\circ$.
The earthquake relocation is based on the method of Sambridge and Kennett (1986) which was implemented in an iterative grid search scheme. The hypocenter locations as given in the EHB catalog are used as initial locations around which a grid is set up of $0.2^\circ \times 0.2^\circ \times$ 20 km with a node spacing of 0.02° and 2 km respectively. Theoretical travel times are computed for each node and observed phase arrival using ak135. Subsequently, theoretical travel times are computed in the 3-D reference velocity model for the corners of the grid with the 3-D ray tracing method of Bijwaard and Spakman (1999a) based on ray perturbation theory. The difference between the travel times using a 3-D and 1-D velocity model is determined at each corner and interpolated onto the other nodes of the grid. By adding the previously computed ak135 travel time to the difference afterwards, 3-D travel times are obtained at each grid node. The interpolation is performed to reduce computation time as 3-D ray tracing for each node and each observed arrival time would significantly increase the task. As criterion for the grid search, a misfit function is minimized, which is here the sum of the squared weighted arrival time residuals (observed arrival time - theoretical arrival time - corrections for ellipticity, station elevation, bounce point topography and water depth for depth phases) at each node. The weights differ by phase type as given in Table 8.1. First, within a time interval of ± 20 s around the origin time, the origin time that produces a minimum misfit is searched. The arrival times are then corrected for the new origin time and the spatial minimum of the misfit function is determined. If the minimum is located near the edge of the grid, the grid

phase type	weight^{-1}
P	0.3
S	1.5
pP, pwP, sP	1.0
PKPdf, PKiKP	1.0

Table 8.1: Weights applied for minimization of the misfit function.

is shifted with the new location as center and the thus found source parameters are used for the following iteration, otherwise the grid is refined to half the node spacing. The relocation procedure is repeated until the node spacing is reduced to 0.005° or when the maximum number of iterations (=6) is reached. On average a final location is found after 3 iterations and only 5% of the events require 6 relocation steps.
The relocations are accepted if the root-mean-square misfit of the residuals is less than the ak135 misfit + 0.5 s and if the epicenter shift is less than 50 km and the depth shift is less than 40 km for free-depth solutions.

8.4 Model

Relocation is performed with a 3-D velocity model obtained from global travel time tomography (named "P06_3Dloc" hereafter). The model was obtained in several processing steps: First, a travel time tomography was performed with travel time residuals from the EHB catalog, EMSC bulletins (Godey *et al.*, 2006) and seismic networks and experiments in North America (Sandoval *et al.*, 2004a) and Europe (Chapter 4) using ak135 as reference model. This model (named "P06") contains many features in the Earth's crust and mantle (e.g. subducting slabs, hot upwellings) in regions of good ray coverage.
Second, the amplitudes of this model were enhanced by doubling the anomaly amplitudes of P06. But in order not to affect the data misfit, only the part of the amplified model was used which lies in the null space. This null space model part was found by applying the null space shuttle of Deal and Nolet (1996). As the resulting model (named "P06$^+$") is a P velocity model, S velocity perturbations were derived using the depth-dependent $d\ln v_s/d\ln v_p$ values of Bolton and Masters (2001) which range from 1.345 in the upper mantle to 3.45 in the lowermost mantle.
Third, the model P06$^+$ was combined with the CUB2.0 model (Ritzwoller *et al.*, 2002b) in the uppermost mantle and the model S20RTS (Ritsema *et al.*, 1999) below that. The CUB2.0 model is based on broadband surface wave group and phase velocity measurements and uses a global crustal model (CRUST2.0, Bassin *et al.*, 2000) in the background. We used the P and S velocities as they are provided in this model. Between 200 and 300 km depth, the model S20RTS was smoothly blent in using a depth-weighted average of both models. S20RTS is based on Rayleigh wave phase velocity measurements, shear wave travel times and normal mode splitting measurements. Since it is a shear velocity model, it was converted to P velocities using the afore mentioned depth-dependent $d\ln v_s/d\ln v_p$ values of Bolton and Masters (2001). P06$^+$ is then combined with CUB+S20RTS applying a hitcount-dependent criterion

where hitcount is the number of rays crossing a model grid-cell. For cells with a hitcount bigger than 500/1000/2000 in the upper/mid/lower mantle P06$^+$ was used. A smooth transition from P06$^+$ to CUB+S20RTS was achieved by using a weighted hitcount-dependent average of both models in an intermediate hitcount range. For cells with a hitcount lower than 100/200/400 in the upper/mid/lower mantle CUB+S20RTS was used. The advantage of this approach is, that in regions of good ray coverage ray bending due to 3-D heterogeneities is accounted for according to P06$^+$ and otherwise according to CUB2.0 or S20RTS respectively which can be assumed to be more realistic models than a 1-D reference model.
Fourth, a final tomography inversion was performed using the extended global data set and CUB+S20RTS+P06$^+$ as reference model. Processing before inversion included a relocation of the earthquakes in the new reference model (similar to the relocation process presented here) to establish consistency between arrival time residuals and source parameters. The resulting model P06_3Dloc combines the long-wavelength structure as "seen" by long period seismic information with the detailed crust and mantle structure obtained from short period travel time data. The conversion to S-velocity anomalies was again performed using the $d \ln v_s / d \ln v_p$ values of Bolton and Masters (2001).

8.5 Location of ground truth events

To find improvements of relocation with the 3-D velocity model, tests with ground truth events are performed. These events are earthquakes and explosions whose source parameters are known exactly. Here, additionally events are considered with a location error up to 5 km. For Eurasia, events are selected from the reference event database of Bondár *et al.* (2004), which were not used for computation of the tomography model. For North America, only ground truth events are available to us, which were also used for tomography. Yet, these events are selected since most of them are located in regions with many stations and events and their influence on the obtained velocity model therefore is minor. For the entire ground truth data set, only events are selected that have a teleseismic secondary azimuth $< 180^\circ$ (i.e. the largest azimuthal region centered around the event containing only one station) and which contain more than 10 teleseismic first arrivals.

8.5.1 Arrival time prediction

Assessment of arrival time prediction with a specific velocity model can indicate its ability to improve earthquake location. Therefore, theoretical arrival times are computed for 58,700 observed P phases of 306 ground truth events (using their exact location) with both ak135 and P06_3Dloc as velocity model. The closer the travel time residuals are to 0 s, the better the velocity model predicts the arrival times. As a summary of the computations, in Figure 8.1 the mean travel time residuals with respect to the epicentral distance are displayed together with their standard deviations. At distances up to approximately 69° the 3-D velocity model predicts the travel times better while between 69° and 76° ak135 gives better results and at greater distances the results are comparable for both models.

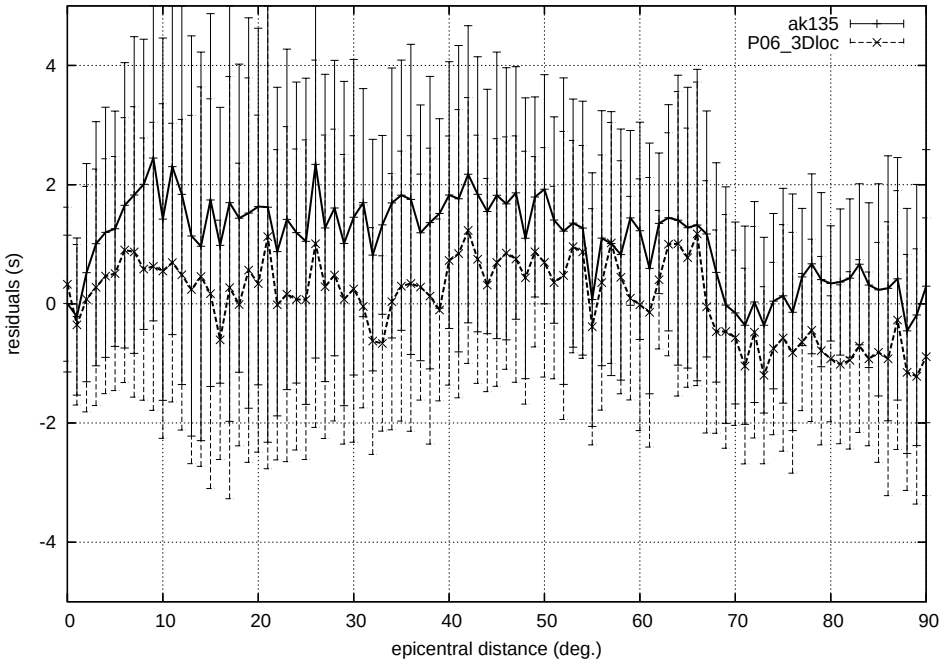

Figure 8.1: Mean travel time residuals and standard deviations computed with ak135 (solid line) and the 3-D velocity model (dashed line) with respect to the epicentral distances for ground truth events in North America and Eurasia.

	epicenter shift (km)	depth shift (km)	origin time shift (s)
fixed depth:			
ak135	9.9 ± 6.7	–	0.7 ± 0.7
3-D	6.4 ± 4.4	–	-0.4 ± 0.6
free depth:			
ak135	9.2 ± 4.8	-7.1 ± 6.9	1.6 ± 1.1
3-D	6.5 ± 4.7	-7.9 ± 6.0	0.8 ± 1.0

Table 8.2: Summary of the mislocations errors obtained for the ground truths events.

8.5.2 Hypocenter location

Mislocation errors are assessed here by relocating the ground truth events. The events are relocated with the method described in Section 8.3 using the 3-D velocity model and, for comparison, they are relocated using ak135 including a correction of the teleseismic travel times for average regional Earth structure below the stations (corrections are applied as provided by Engdahl *et al.* (1998)). Only the best constrained events are analyzed, which involve more than 250 phases for relocation and have a depth shift smaller than 40 km and a epicenter shift smaller than 50 km. The absolute origin time shift is restricted to 3.5 s to exclude events that do not contain sufficient depth-defining phases and therefore cause large trade-offs between depth and origin time shifts.
Thus, 226 events are relocated fixing the depth to the true location and 93 events are relocated allowing the hypocenter depth to shift. For the fixed-depth solutions using the 3-D velocity model and ak135 (including patch correction) respectively, relocation vectors are displayed in Figure 8.2. The relocation vectors are smallest in North America and parts of the Mediterranean region, which suggests that the events in those regions are well-constrained by travel time observations and/or that the 3-D model provides a good representation of Earth structure in those regions. As the event locations are known with an accuracy of 0-5 km, the source parameter shifts can be considered as mislocation errors. These mislocation errors are given in Table 8.2 for fixed- and free-depth solutions using ak135 and the 3-D velocity model. The fixed-depth solutions display epicenter shifts similar to the free-depth solutions and the mislocations are bigger for ak135 than for P06_3Dloc. The depth shift of the free-depth solutions is smaller for ak135 than P06_3Dloc but only suitable ground truth events with a focal depth < 35 km were found. Therefore, the depth mislocation might not be representative for deeper events. As can be expected due to a trade-off between origin time and event depth shift, the origin time shift is smaller for the fixed-depth solutions than the free-depth solutions and in both cases the origin time error is smaller for the 3-D model than ak135.
In summary, as arrival time prediction is improved due to the 3-D velocity model, relocation with that model reduces source location errors.

8.6 Results of relocating the global hypocenter data set

The relocation of 450,000 events took 2433 CPU-hours on an SGI Altix system using 8 Itanium-2 processors. It resulted in 203,000 events with a fixed-depth solution and 247,000

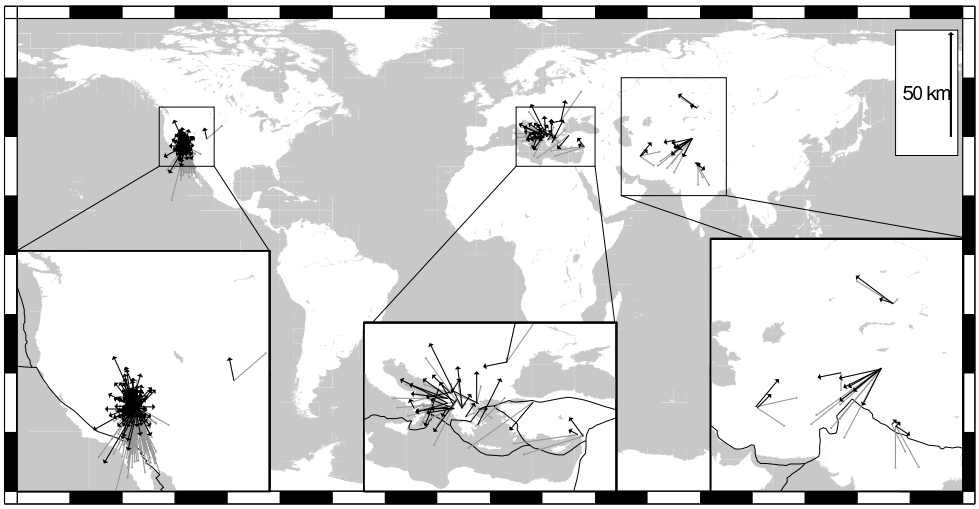

Figure 8.2: Relocation vectors of the ground truth events using the 3-D velocity model (black) and using ak135+patch correction (gray). The vector tails indicate the ground truth locations. The length of the relocation vectors is exaggerated with the length scale for the global plot as indicated.

events with a free-depth solution of which 187,000 and 232,000 relocations respectively were accepted. The rest was discarded as the event parameters were not well enough constrained by arrival time observations and therefore deviated too much from the initial location (constraints given in Section 8.3).
A summary of the source parameter shifts with respect to the original parameters using ak135 as velocity model for events with more than 10 travel time residuals is given in Table 8.3 and illustrated in Figure 8.3. For most of the accepted events the epicenter shift is less than 20 km and it amounts on average to 12.8 km. Also, the epicenter shifts for both fixed-depth and free-depth events increase with depth. For most of the free-depth events the depth shift is less than 15 km with an average shift of -3.1 km. The depth shifts are largest for shallow events and decrease with depth as model anomalies are largest in the crust and decrease with depth. Furthermore, the origin time shift is centered around 0.0 s and most events show an origin time shift of less than ± 2 s. The root-mean-square values of the travel time residuals after relocation with respect to the residuals obtained with ak135 are mainly unchanged or decrease by $\lesssim 0.5$ s with an rms misfit of less than 3 s for the majority of events (see Fig. 8.4).
In Figures 8.5 and 8.6 characteristic features of the relocations are illustrated by zooming in on the region where the Pacific plate is subducted to the west underneath the Eurasian and Philippine plates (top), the eastern plate boundaries of the Cocos and Nazca plates that are subducted underneath the Caribbean and South American plate (middle) and the plate boundary between Africa and Europe in the eastern Mediterranean Sea (bottom).
For East Asia only earthquakes with an EHB hypocenter depth > 70 km are displayed to allow for better visualization. Along the western Pacific plate boundary, mainly negative ori-

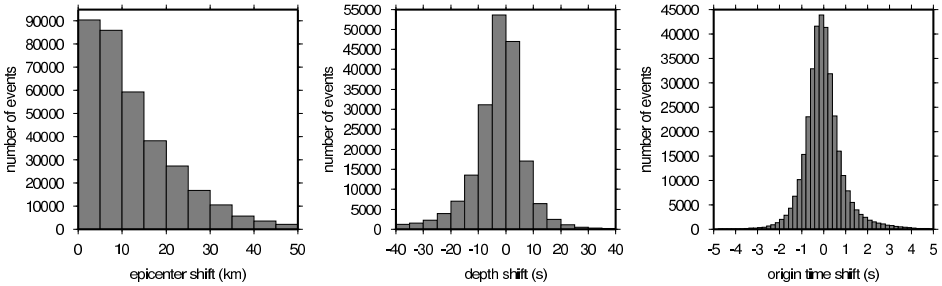

Figure 8.3: A histogram of the epicenter shifts with respect to the original ak135 locations (including patch corrections) for fixed- and free-depth events (left), a histogram of the depth shift for free-depth events (middle) and a histogram of the origin time shift for fixed- and free-depth events (right).

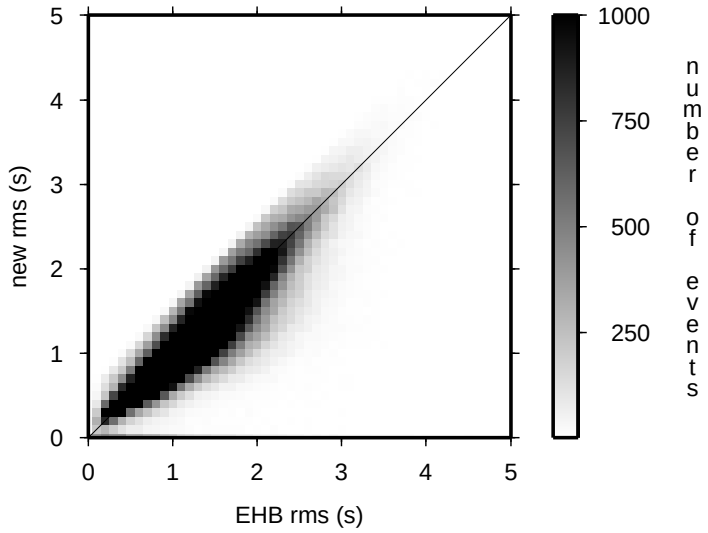

Figure 8.4: Density plot of the root-mean-square data misfit before (ak135 residuals) and after (3-D residuals) relocation.

gin time shifts can be observed. They compensate for remaining data misfit not accounted for by computation of travel time residuals with the 3-D reference model. Close to Japan and along the Mariana trench the epicenter shifts are comparatively small (≈ 20 km) as the events are well-constrained and point towards the trench taking into account the existence of a high-velocity slab anomaly in the subduction zone.
Along the Andean subduction zone, origin time shifts are also mostly negative around -1 s in the southern Altiplano region decreasing significantly in the deeper parts of the subducted slab to ± 0 s while origin time shifts to the north are larger, between -2 s and -1 s. The epicenter shifts are on the order of 25–30 km in the Altiplano region pointing, like in the eastern Pacific subduction zones, towards the trench. North of the Altiplano plateau and at greater depth the relocation vectors are generally smaller, particularly the deep events have relocations of less than 10 km.
Along the southern part of the Middle American trench, the origin time shifts are generally negative and epicenter shifts are large moving the events northwestward in the northern part of the subduction zone while they shift the epicenters towards the trench in the southern part. In the eastern Caribbean origin time and epicenter shifts are mostly smaller relocating the earthquakes again towards the trench.
Relocation in the Aegean area shows many variations as the tectonic settings in which earthquakes occur are complex. Furthermore, most events in this region are located at shallow depth. In the Tyrrhenian basin, small negative origin time shifts are observed with small relocation vectors preserving the event clustering. Near Crete in the Aegean subduction zone, positive origin time shifts are found that change into small negative origin time shifts indicating the difference in source depth and model properties in this region. They are accompanied by small epicenter shifts showing that the locations are well-constrained by the travel time observations for these earthquakes. In the Vrancea region in Romania, where plate subduction took place along the Carpathian arc, negative origin time shifts indicate reduction of data misfit due to correction of the source parameters regarding the high-velocity slab there. Otherwise, epicenter and depth shifts in this region are small keeping the clustering of events within this very limited region.
As illustrated in Figure 8.6, in well-sampled regions as the subduction zone across Japan, depth and epicenter shifts are small leaving the locations almost unchanged. Also in South America, earthquake locations in the slab are only relocated over small distances. However, below 150 km depth the events are more clustered now narrowing the region in which seismicity is observed. In the Mediterranean where most earthquakes occur at shallow depth, events at less than 50 km depth are mainly located downwards building a layer of approximately 20 km thickness in which they cluster. Again, deeper events around 150 km depth are more focussed after relocation at the top of the slab.

8.7 Conclusions

We relocated a global earthquake data set with a 3-D reference model to account for local heterogeneities in the sources regions which could not be accounted for in the preceding relocation by Engdahl *et al.* (1998). As tests with ground truth events show, the 3-D reference model predicts travel times particularly at regional distances better than ak135. Furthermore,

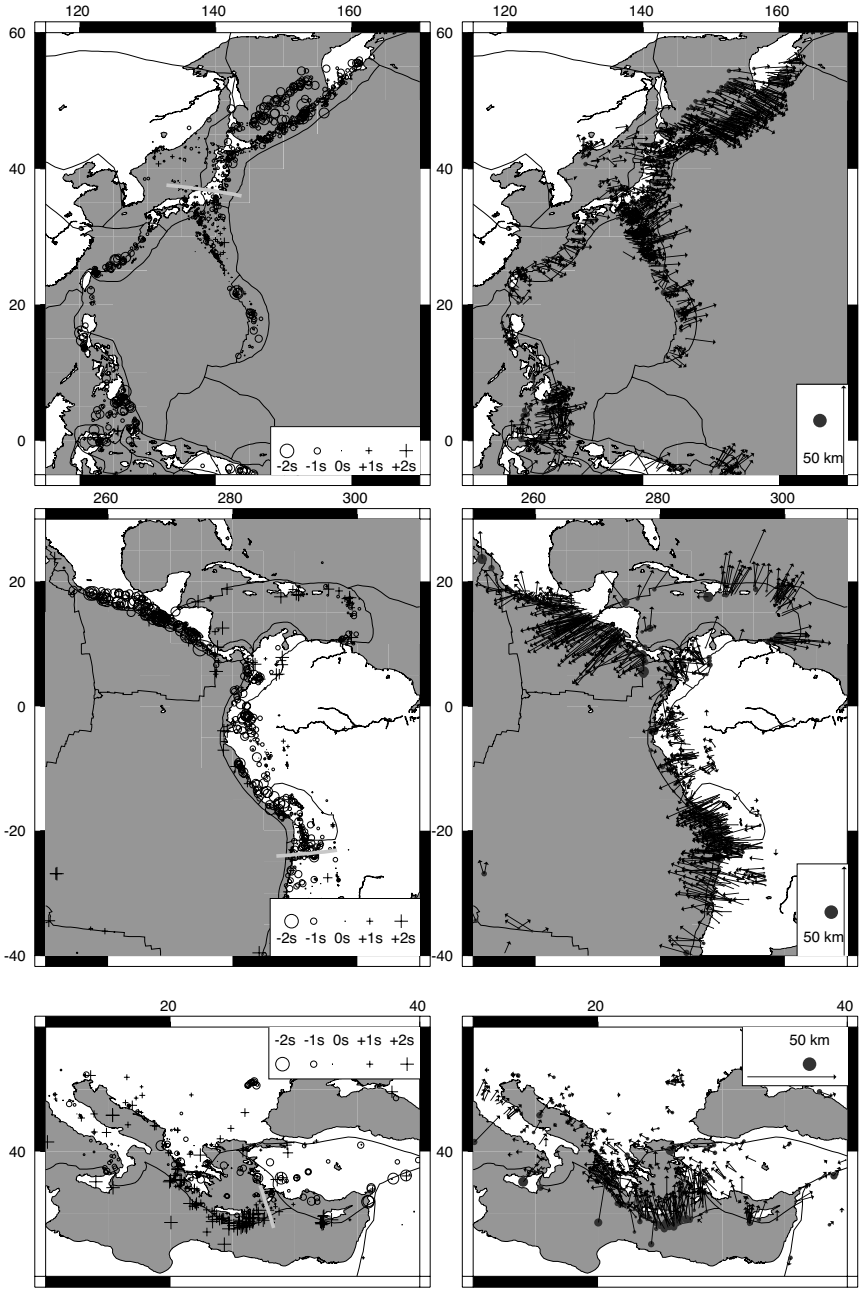

Figure 8.5: Source time shift (left) and epicenter shift (right) with respect to the original locations using ak135 as velocity model in the area of the Philippine plate (top), along the Cocos and Nazca plate subduction zones (middle) and in the eastern Mediterranean basin (bottom). For better visualization, in the top panels only events with more than 250 travel time residuals and an EHB focal depth > 70 km are displayed, in the other panels earthquakes at all depths are displayed but only those with > 250 travel time residuals in the mid panels and > 350 in the bottom panels.

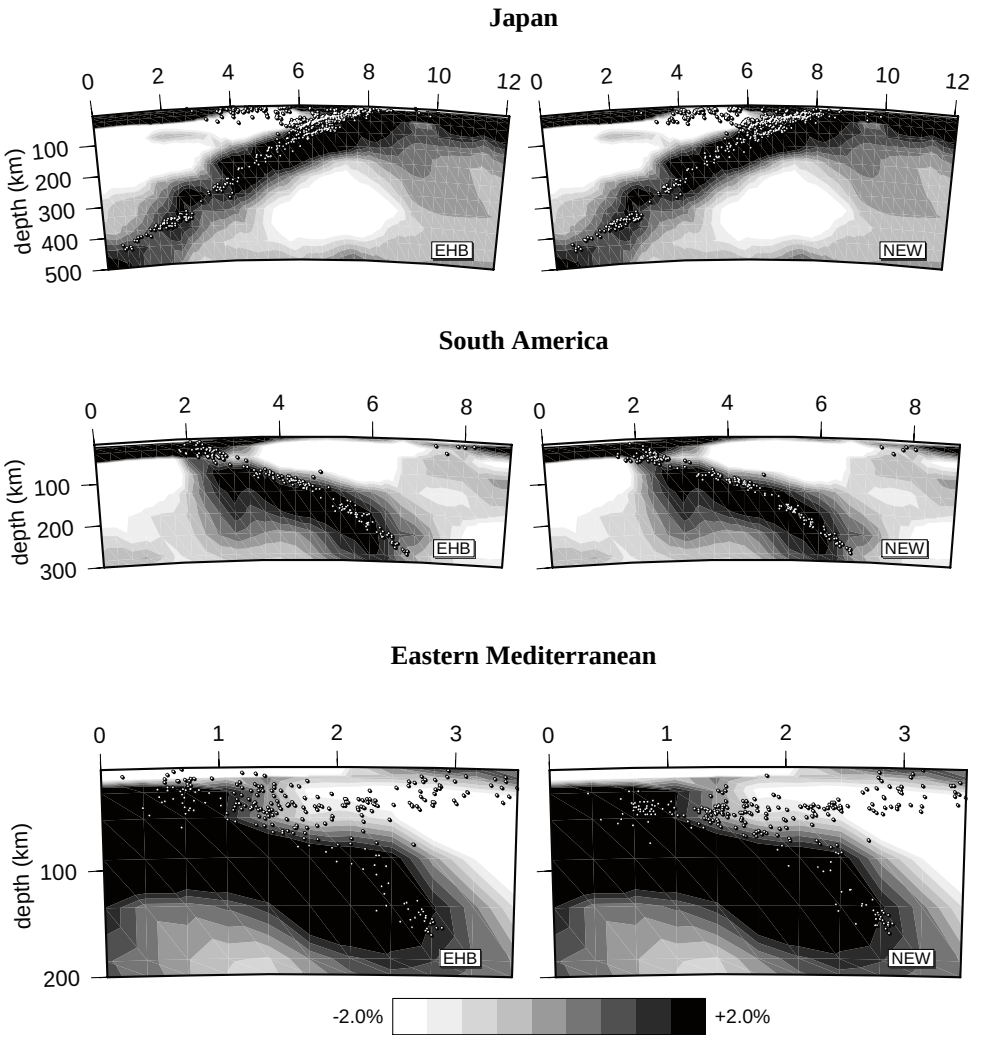

Figure 8.6: Vertical cross sections of three subduction zones. White dots represent the original locations using ak135 as reference model (left column) and new locations (right column). Displayed are free-depth events with more than 150 registrations for a slice of $\pm 2.0^\circ$ width. The location of the slices is marked with gray lines in Figure 8.5. The grayscales in the background display the P06_3Dloc model anomalies along the cross section. Black tones represent velocities that are higher than the corresponding ak135 velocity at that depth and white tones indicate lower velocities.

	initial depth range			
	all	< 70 km	70 km–300 km	≥ 300 km
epicenter shift (km):				
fixed-depth events	12.8 ± 12.8	11.8 ± 12.7	17.4 ± 11.8	22.2 ± 9.7
free-depth events	12.8 ± 11.0	12.4 ± 11.6	12.9 ± 9.7	17.4 ± 9.3
all events	12.8 ± 11.8	12.0 ± 12.2	14.1 ± 10.5	19.1 ± 9.7
depth shift (km):				
fixed-depth events	–	–	–	–
free-depth events	-3.1 ± 9.4	-4.4 ± 9.8	-0.6 ± 7.9	-0.6 ± 8.2
all events	–	–	–	–
origin time shift (s):				
fixed-depth events	-0.1 ± 0.7	-0.1 ± 0.7	0.0 ± 0.6	-0.2 ± 0.5
free-depth events	0.1 ± 1.1	0.2 ± 1.2	-0.1 ± 0.7	-0.1 ± 0.7
all events	0.0 ± 0.9	0.0 ± 1.0	-0.1 ± 0.7	-0.1 ± 0.6

Table 8.3: Average source parameter shifts and rms-scatter of the accepted relocations with respect to the initial location for different depth ranges.

relocation with the 3-D velocity model gives smaller epicenter mislocations and the origin time errors are reduced, only the depth mislocations are slightly increased. However, for the estimation of the depth mislocation only surface and crustal ground truth events exist and relocation of the global hypocenter data set shows that depth shifts below the crust are significantly reduced suggesting that also the depth mislocation errors are reduced for deeper located events.
Besides that, the results show that relocation with theoretical travel times computed in the 3-D velocity model agree well with the computations using ak135 + regional patch corrections as the overall source parameter shifts are small. The relocations mainly account for 3-D velocity structure which could not be taken into account by the patch corrections in the computation of Engdahl *et al.* (1998) as systematic location changes indicate. Thereby, subduction-related epicenters are relocated towards the trench and remaining data misfit after consideration of the 3-D velocity model is accounted for by negative origin time shifts. At shallower depth, the earthquakes are mainly located downwards and origin time shifts vary as the crust of the 3-D model changes locally. Overall, more focussing of the earthquakes in clusters is obtained, particularly at depths greater than 150 km.

8.8 Acknowledgments

We thank the ISC, NEIC, EMSC, ANSS, ORFEUS, CNSN, IRIS, SCEDC, Stephen Arrowsmith, the CALIXTO, EIFEL, MIDSEA, NARS-Baja, SVEKALAPKO and TOR working groups for providing the data used in this study. Computational resources for this work were provided by the EUROMARGINS programme of the European Science Foundation (01-LEC-MA22F WESTMED) and by the Netherlands Research Center for Integrated Solid Earth Science (ISES 3.2.5 High End Scientific Computation Resources).